Clim Dyn (2017) 49:4293–4310
DOI 10.1007/s00382-017-3534-z

Observed and CMIP5 modeled influence of large-scale circulation on summer precipitation and drought in the South-Central United States

Jung-Hee Ryu[1] · **Katharine Hayhoe**[1,2]

Received: 11 August 2016 / Accepted: 10 January 2017 / Published online: 3 February 2017

Abstract Annual precipitation in the largely agricultural South-Central United States is characterized by a primary wet season in May and June, a mid-summer dry period in July and August, and a second precipitation peak in September and October. Of the 22 CMIP5 global climate models with sufficient output available, 16 are able to reproduce this bimodal distribution (we refer to these as "BM" models), while 6 have trouble simulating the mid-summer dry period, instead producing an extended wet season ("EW" models). In BM models, the timing and amplitude of the mid-summer westward extension of the North Atlantic Subtropical High (NASH) are realistic, while the magnitude of the Great Plains Lower Level Jet (GPLLJ) tends to be overestimated, particularly in July. In EW models, temporal variations and geophysical locations of the NASH and GPLLJ appear reasonable compared to reanalysis but their magnitudes are too weak to suppress mid-summer precipitation. During warm-season droughts, however, both groups of models reproduce the observed tendency towards a stronger NASH that remains over the region through September, and an intensification and northward extension of the GPLLJ. Similarly, future simulations from both model groups under a +1 to +3 °C transient increase in global mean temperature show decreases in summer precipitation concurrent with an enhanced NASH and an intensified GPLLJ, though models differ regarding the months in which these decreases are projected to occur: early summer in the BM models, and late summer in the EW models. Overall, these results suggest that projected future decreases in summer precipitation over the South-Central region appear to be closely related to anomalous patterns of large-scale circulation already observed and modeled during historical dry years, patterns that are consistently reproduced by CMIP5 models.

Keywords Precipitation · Drought · Southern Plains · South Central U.S. · North Atlantic Subtropical High · Great Plains low-level jet · Global climate models · CMIP5

1 Introduction

The South-Central (SC) United States is characterized by a strong east-to-west precipitation gradient that results in highly diverse climate zones, from the coastal wetlands of the Gulf Coast to the agricultural semi-arid plains of West Texas. Throughout this region, precipitation is driven by a complex set of features that span a broad spectrum of temporal and spatial scales, from mesoscale convective systems to synoptic-scale fronts, mid-latitude storms, and hurricanes. In recent years, extreme precipitation deficits combined with record high temperatures have led to record-breaking droughts that have impacted water availability, crop and rangeland productivity, human health, and the economy (Fannin 2012; Basara et al. 2013). For example, the 2011 drought and heat wave caused over $12B in damages and 95 deaths across the Southern Plains including Texas, Oklahoma, and New Mexico (NCDC 2013) while in 2014, the USDA designated 588 drought-stricken counties

Electronic supplementary material The online version of this article (doi:10.1007/s00382-017-3534-z) contains supplementary material, which is available to authorized users.

✉ Jung-Hee Ryu
jung-hee.ryu@ttu.edu

[1] Climate Science Center, Texas Tech University, MS1015, Lubbock, TX 79409, USA

[2] Department of Political Science, Texas Tech University, Lubbock, TX 79409, USA

covering nearly the entire West and Southern Great Plains (USDA 2015).

Planning for the impacts of global climate change on extreme heat and drought risk represents a significant challenge for resource managers and policy makers throughout this region. Observed trends and future projections suggest that, although annual precipitation may not change significantly in the SC region, climate change is likely to affect the frequency and severity of future heat waves and growing season drought risk, with more frequent heat waves (Barriopedro et al. 2011) and increased risk of spring and summer precipitation deficits (Hoerling et al. 2013; Shafer et al. 2014; Garfin et al. 2014) that scale with global mean temperature (Swain and Hayhoe 2015). While modeled precipitation depends on a complex mix of the physical parameterizations used to represent convective processes, boundary-layer processes, and land-surface interactions, the large-scale circulation features that drive variability and trends in regional precipitation and drought risk occur at spatial scales resolved by climate models. Therefore, examining how climate models reproduce these patterns and their relationship to precipitation variability and drought, and the extent to which future changes in precipitation and drought risk are linked to shifts in large-scale patterns, may provide insight into projected future change.

A key large-scale dynamical feature that affects summer precipitation over much of the U.S. is the North Atlantic Subtropical High (NASH), a semi-permanent anti-cyclonic system dominating the lower troposphere over the North Atlantic (Davis 1997). While the NASH has been shown to strongly influence warm season precipitation variability over the southeastern U.S. at seasonal, interannual and decadal scales (Henderson and Vega 1996; Diem 2006; Li et al. 2011; Ortegren et al. 2011), Henderson and Muller (1997) suggest that the westward expansion of the Atlantic subtropical high also affects summer surface climate variability in the South Central region. A westward extension of the NASH could affect precipitation by setting up and maintaining a prevailing high pressure system, resulting in moisture flux divergence and mid-tropospheric stability that in turn suppresses convective activity over the region. Its relevance to drought is emphasized by many other observational analyses that have demonstrated how the 1930s, 1950s, and 1980s Great Plains droughts were characterized by anomalous anti-cyclonic circulation over the region (Namias 1955, 1982; Klein 1952; Dickson 1980). In terms of long-term trends, Li et al. (2012) also found that a westward shift in the NASH has become more frequent in recent decades, associated with anthropogenic forcing as well as internal climate variability such as the Pacific Decadal Oscillation (PDO). In previous work, however, we found that CMIP5 models vary in their ability to simulate the timing and magnitude of annual variations in the NASH, with implications for model ability to simulate the cycle of annual precipitation in the Caribbean and moisture transport throughout the Gulf of Mexico region (Ryu and Hayhoe 2014).

The Great Plains Low-Level Jets (GPLLJ) is another large-scale dynamical feature that affects summer precipitation in the South Central region, through moisture transport from the Gulf of Mexico and jet-induced low-level convergence (Higgins et al. 1997; Mo et al. 2005; Cook 2008; Weaver and Nigam 2008; Weaver et al. 2009; Ruiz-Barradas and Nigam 2013). The GPLLJ is a supergeostrophic wind that arises from the spatially uneven heating of sloping terrain over the eastern Rocky Mountains and boundary layer frictional effects (Blackadar 1957; Wexler 1961; Holton 1967; Bonner and Paegle 1970; Hoxit 1975). Although the GPLLJ is primarily nocturnal, it is still distinct at the monthly scale as its southerly winds advect moisture from the Gulf of Mexico over the continental U.S. (Helfand and Schubert 1995; Davis et al. 1997; Higgins et al. 1997). In terms of its influence on precipitation variability across the Great Plains, the GPLLJ's moisture transport dominates over local evaporation (Ruiz-Barradas and Nigam 2005), influencing both wet and dry precipitation extremes, including the 1988 drought and the 1993 floods (Ting and Wang 2006; Cook et al. 2008; Weaver and Nigam 2011). The GPLLJ is also affected by large-scale factors such as the westward extension of the NASH (Rodwell and Hoskins 2001). In terms of long-term trends, Barandiaran et al. (2013) have documented a strengthening and northward extension of the GPLLJ from 1979 to 2012, with concurrent decreases in precipitation across the southern Great Plains. Future projections suggest that the GPLLJ could intensify under anthropogenic forcing, reducing precipitation in the southern Great Plains, while increasing it to the north (Cook et al. 2008).

Future projections from regional climate model simulations forced by boundary conditions from both previous- and present-generation coupled global climate models (CMIP3 and CMIP5) show decreases in warm season rainfall in the Southern Plains (Patricola and Cook 2013a, b; Harding et al. 2013; Harding and Snyder 2014) related to a strengthening of the GPLLJ accompanied by an intensification of the western portion of the NASH. Other recent studies emphasize the importance of large-scale drivers such as the NASH in driving warm season precipitation and dry spells in the central and southern U.S. (Wuebbles et al. 2014; Li et al. 2015; Zhao et al. 2016). Aiding in the interpretation of this work, Harding et al. (2013) concluded that the ability of regional climate models to accurately simulate precipitation over the Great Plains is closely related to the performance of the CMIP5 models providing the boundary conditions for the downscaling, particularly

their ability to simulate the Atlantic Warm Pool as well as central U.S. precipitation.

Here, we build on the results of these previous studies to examine the ability of a comprehensive ensemble of all available output from atmosphere-only and coupled CMIP5 model simulations to simulate the climatological annual cycle of precipitation and its link to the NASH and GPLLJ in both historical and future simulations, with a focus on warm-season precipitation and drought. Through analyzing such a large ensemble of models, we specifically seek to determine whether model ability to reproduce the observed historical influence of large-scale circulation patterns on regional precipitation affects projected changes in warm-season precipitation and drought risk. In other words, does precipitation and summer drought risk respond differently to future anthropogenic forcing in models that are able to connect historical NASH and GPLLJ variations to precipitation, as compared to in models that can't? In examining this large ensemble of simulations, we also seek to extend the work of Patricola and Cook (2013b) to determine whether projected decreases in summer precipitation in the Southern Great Plains is generally related to a strengthening of the GPLLJ accompanied by an intensification of the western portion of the NASH in all coupled model simulations, or whether this is only a feature of models that are able to reproduce the observed relationship between these large-scale circulation features and warm-season precipitation. In pursuing these questions, we seek insight regarding the robustness of large, multi-model ensemble projections of changes in drought risk and warm-season precipitation over the Southern Great Plains.

Our study area includes Texas, Oklahoma, Kansas, Missouri, Arkansas, and Louisiana, and is bounded by a rectangle from 103 to 92°W and 28 to 40°N, as shown in Fig. 1. Using gridded observations and reanalysis data, we first examine how the NASH and GPLLJ are related to the

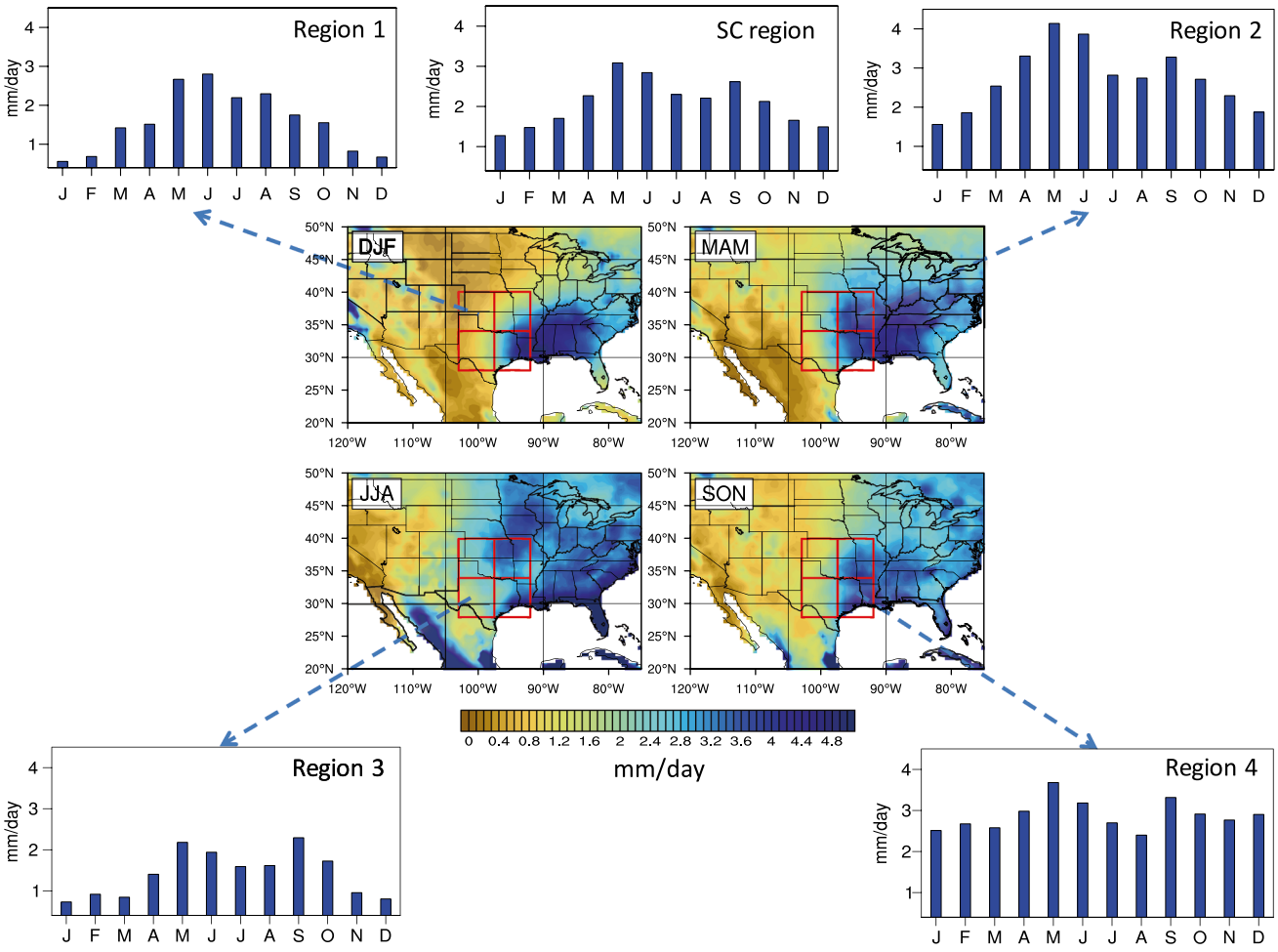

Fig. 1 Spatial distribution of U.S. continental seasonal mean precipitation from 1979 to 2008 (*center*) and the climatological annual cycle averaged over four sub-regions marked with *red boxes*; *Region 1* (97.5–103°W/34–40°N, *top-left*), Region 2 (92–97.5°W/34–40°N, *top-right*), Region 3 (97.5–103°W/28–34°N, *bottom-left*), and Region 4 (92–97.5°W/28–34°N, *bottom-right*). Climatological annual precipitation cycle averaged over the entire SC region is shown in the *top-center plot*

month-to-month variations in the climatological annual cycle of precipitation, and how their anomalous behavior affects precipitation during historical droughts. We next assess the ability of global climate models to reproduce the observed relationships between climatological and interannual precipitation and the NASH and GPLLJ. Finally, we examine the relationship between projected changes in warm-season precipitation and changes in large-scale dynamics under a range of future scenarios, and the extent to which these long-term trends in response to anthropogenic forcing reflect the patterns observed during historical droughts.

2 Data and model output

Gridded monthly precipitation at a resolution of 0.5° × 0.5° latitude and longitude was obtained from the Climate Research Unit Time Series (CRU TS) version 3.23. This dataset integrates observations from 1901 to 2014 from over 4,000 stations records across the globe (Harris et al. 2014). We also used precipitation from the North American Regional Reanalysis (NARR), a long-term set of high-resolution (32 km) gridded reanalysis output from 1979 through near present (Mesinger et al. 2006), as it assimilates rain gauge data for improved representation of precipitation over the U.S., particularly nocturnal precipitation over the Plains associated with the GPLLJ (Bukovsky and Karoly 2007). For the large-scale dynamical analysis, we used NARR monthly mean geopotential height, zonal and meridional wind from 1979 to 2012, focusing on 700 hPa geopotential height to depict the NASH and 925 hPa meridional wind for the GPLLJ.

Monthly precipitation and vertically-resolved atmospheric variables were also obtained from global climate models participating in phase 5 of the Coupled Model Intercomparison Project (CMIP5; Taylor et al. 2012). We use atmosphere-only AMIP experiments where sea ice and surface temperature are determined by observations rather than model simulations, and coupled CMIP experiments where the entire climate system, including atmosphere, ocean, and cryosphere, is allowed to respond directly to observed anthropogenic and natural inputs. For the large-scale dynamical analysis, we required monthly geopotential height and zonal and meridional wind as well as 2 m daily maximum and mean air temperature and precipitation, and used all available models that had the outputs required for this analysis. This included AMIP simulations from 14 different models and 12 different institutions, and CMIP simulations from 22 different models and 13 different institutions, all of which were archived by CMIP5.

A brief description of the models used in this study, including their names, provenance, and horizontal resolution, is provided in Table 1. For the present-day analysis, we used model outputs for 30 years, beginning in 1979, in order to cover the same period for which NARR output is available. These "historical" simulations correspond to historical total-forcing simulations (Taylor et al. 2012) from 1979 to 2005 and the Representative Concentration Pathway (RCP) 4.5 scenario from 2006 to 2008 (Moss et al. 2010).

To analyze the projected future changes in precipitation and large-scale circulation features that would occur under a given global mean temperature target, we began with CMIP5 simulations by the 22 models listed in Table 1 using RCP higher (8.5) and lower (4.5) scenarios for the period 2006 to 2100. For each individual simulation, we identified the first 20-year period for which area-weighted global mean 2 m temperature increases by +1, +2, and +3 °C relative to the present (1971–2000) climatology. The timing of the first period when global mean temperature reaches each threshold varies according to each model, scenario, and simulation; this method is described in more detail in Swain and Hayhoe (2015) and an explanatory figure and text is included in the Supplemental Materials. Each 20-year period was then used to identify the output from each model/scenario combination to be averaged to calculate the ensemble mean change for each global mean temperature threshold.

3 Annual precipitation climatology

3.1 Observations

Figure 1 (center) shows the spatial distribution of seasonal mean precipitation over the central U.S. for a 30-year climatology from 1979 to 2008, derived from the CRU gridded station data. The South Central region, as indicated by the red box, is characterized by a strong west-east gradient and seasonal cycle, with wetter conditions in summer and drier in winter. Closer examination (Fig. 1, top) shows that climatological annual cycle of the SC region has a weak bimodal distribution, with a wet season from May through September that can be divided into a maximum in May and June and a second maximum in September and October, punctuated by a mid-summer dry period in July and August.

Dividing the SC region into four sub-regions shows that this bimodal feature is strongest in the southeast, and weakest in the northwest, part of the region (Fig. 1, corners). Beginning with northern Texas and eastern Oklahoma and Kansas, Region 1 is relatively dry, with annual mean precipitation of 1.6 mm/day and a continuous wet season from May through August. Region 2, covering the eastern halves of Oklahoma and Kansas and some of Missouri and

Table 1 A description of the CMIP/AMIP models used in this analysis, including their names, institutes, and horizontal resolution (approximate degrees in longitude and latitude) of atmospheric models

Modeling center	Models	Resolution (atmosphere)
Beijing Normal University, China	BNU-ESM*	T42 (2.8°)
Center for Climate System Research (University of Tokyo), National Institute for Environmental Studies, and Frontier Research Center for Global Change (JAMSTEC), Japan	MIROC5*	T85 (1.4°)
	MIROC-ESM*	T42 (2.8°) w/carbon cycle
	MIROC-ESM-CHEM	T42 (2.8°) w/ carbon cycle + chemistry
Centre National de Recherches Meteorologiques/Centre Europeen de Recherche et Formation Avancees en Calcul Scientifique	CNRM-CM5*	T127 (1.4°)
Commonwealth Scientific and Industrial Research Organization (CSIRO) and Bureau of Meteorology (BOM), Australia	ACCESS1-0*	1.875° × 1.25°
	ACCESS1-3*	1.875° × 1.25°
CSIRO (Commonwealth Scientific and Industrial Research Organisation, Australia), and BOM (Bureau of Meteorology, Australia)	CSIRO-Mk3.6.0	T63 (1.9°)
Geophysical Fluid Dynamics Laboratory (GFDL), USA	GFDL-CM3*	2.5° × 2.0°
	GFDL-ESM2M	
Hadley Centre for Climate Prediction and Research/Met Office, UK	HadGEM2-AO/HadGEM2-A*	1.875° × 1.25°
	HadGEM2-CC	
	HadGEM2-ES	
Max Planck Institute for Meteorology, Germany	MPI-ESM-LR*	T63 (1.9°)
	MPI-ESM-MR*	
Meteorological Research Institute, Japan	MRI-CGCM3*	TL159 (1.1°)
National Aeronautics and Space Administration (NASA)/Goddard Institute for Space Studies (GISS), USA	GISS-E2-H	2.5° × 2.0°
	GISS-E2-R*	
National Center for Atmospheric Research, USA	CCSM4*	1.25° × 1°
National Science Foundation, Department of Energy, National Center for Atmospheric Research	CESM1(BGC)	1.25° × 1°
	CESM1(CAM5)*	
Norwegian Climate Centre, Norway	NorESM1-M*	2.5° × 1.9°

The models of which the AMIP experiment output are utilized in this study are marked with asterisk

Arkansas, is the wettest part of the domain, with annual mean precipitation of about 2.9 mm/day. Its strongest precipitation peak is in May and June, with a much weaker second peak in September and October. Region 3 includes mostly the west and central Texas. It is the driest region in the domain, with an annual mean of about 1.5 mm/day. Its annual cycle features two nearly equal precipitation peaks punctuated by a distinct mid-summer dry period in July and August. Finally, Region 4, encompassing eastern Texas and Louisiana, has the most distinct bimodal pattern, with two distinct peaks and a very dry period in July and August. It is also the wettest part of the region, with annual mean precipitation of about 3.1 mm/day.

To further quantify the annual cycle of the spatially coherent pattern of the precipitation across the SC region, we conducted a principal component analysis of the 30-year monthly precipitation after Kutzbach (1967). As shown in Fig. 2, the first two EOFs explain about 47% of total variance. The first EOF, that accounts for 30% of total variance, is positive across the entire SC region and its time series is characterized by a familiar bimodal pattern with a mid-summer dry period in July and August, consistent with the climatological annual cycle of the precipitation shown in Fig. 1 (top). The second EOF explaining about 17% of total variance is related to the variation of cold season precipitation in the eastern Texas, Louisiana and Arkansas and warm-season precipitation in northern Texas, Oklahoma, and Kansas. It is consistent with Fig. 1 in that Region 4 is relatively wet during the cold season, and Region 3 is less dry during the warm season compared to other regions.

3.2 Historical CMIP5 simulations

In Fig. 3, we next compare the annual climatological precipitation cycle from gridded observations with NARR, AMIP and CMIP simulations. Compared to observations, it can be seen that the NARR distribution is not as strongly bimodal; in the Supplementary Information we show this is unique to NARR by comparing NARR to two additional observational datasets. In terms of the magnitude of precipitation, it is obvious that the AMIP simulations tend to underestimate precipitation amounts during the wet season, and the second peak in September and October is barely discernible in the AMIP experiments (Fig. 3a). In contrast,

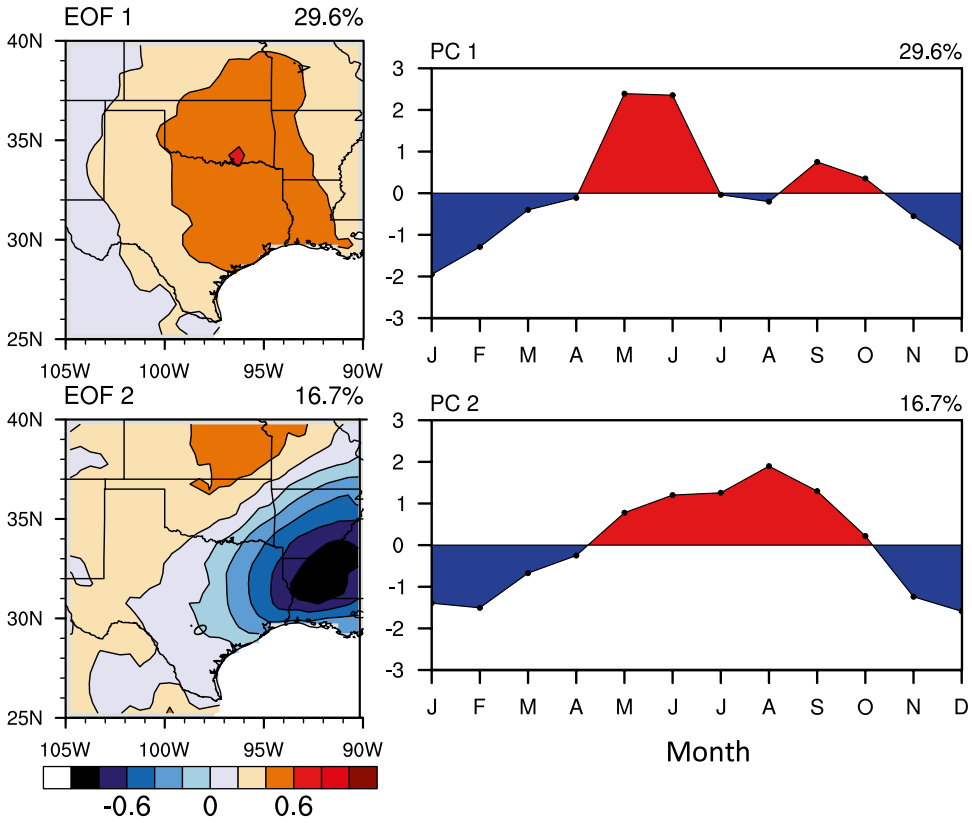

Fig. 2 *Left* spatial patterns of the first two EOF modes associated with monthly precipitation over the SC region from 1979 to 2008 based on CRU data. *Right* principal components corresponding to each EOF mode are plotted after averaging each month's values for 30 years to represent the recurring annual pattern of each EOF mode

CMIP simulations are better able to simulate precipitation amounts during the wet season (Fig. 3b), producing results that more closely resemble both observed gridded and reanalysis data. This result is interesting in that sea surface temperature, one of primary components influencing atmospheric circulation, is prescribed in the AMIP experiments but simulated in CMIP experiments. Assuming that the physical parameterizations related to precipitation do not significantly differ between the AMIP and CMIP experiments of each model, it appears that atmosphere bias in the AMIP experiments might be mediated by the local and remote influence of simulated SST in CMIP experiments. Further investigation into the origins of the AMIP bias and the response to simulated SST in the CMIP simulations is needed, but lies beyond the scope of this paper.

When precipitation cycles are normalized, it is clear that the wet season tends to begin about a month early in both experiments (Fig. 3c, d). As a result, both AMIP and CMIP simulations overestimate precipitation in April, a time when net shortwave radiation at the surface increases rapidly to near summer values. Previous studies have reported that convective parameterizations employed in climate models tend to strongly respond to surface forcing, which results in the diurnal cycle of the simulated precipitation over land having a peak at or near noon, unlike observed precipitation which peaks in late afternoon and nighttime in the Great Plains (Betts et al. 1996; Bechtold et al. 2004; Dai 2006; Dirmeyer 2012). Combining these findings with the bias shown in Fig. 3c, d suggests that an overly-strong response of modeled convective parameterization to surface heating could be responsible for the early onset of the wet season in both experiments; further discussion of this hypothesis is provided in the Supplementary Information, as this study focuses primarily on the summer season.

Based on model ability to simulate the bimodal annual cycle of precipitation in the South Central region in CMIP simulations, we divide the models into two groups: those that are able to reproduce a bimodal distribution ("BM" models), and those that have an extended wet season through July and August ("EW" models). As indicated in Fig. 4a, BM models are able to simulate a mid-summer dry period in July and August and a weak second peak in September and October, although summer rainfall tends to be underestimated compared to both NARR and CRU data. In contrast, EW models tend to overestimate summer rainfall, particularly in July and August, resulting in a single extended wet season, rather than a bimodal distribution (Fig. 4b).

The inverse relationship between warm-season surface temperature and precipitation in the US Great Plains is well-known: when it's wet, it's cool and when it's dry, it tends to be hot (Madden and Williams 1978; Chang and Wallace 1987; Durre et al. 2000). Most CMIP models tend to have a cold bias in daily maximum temperature

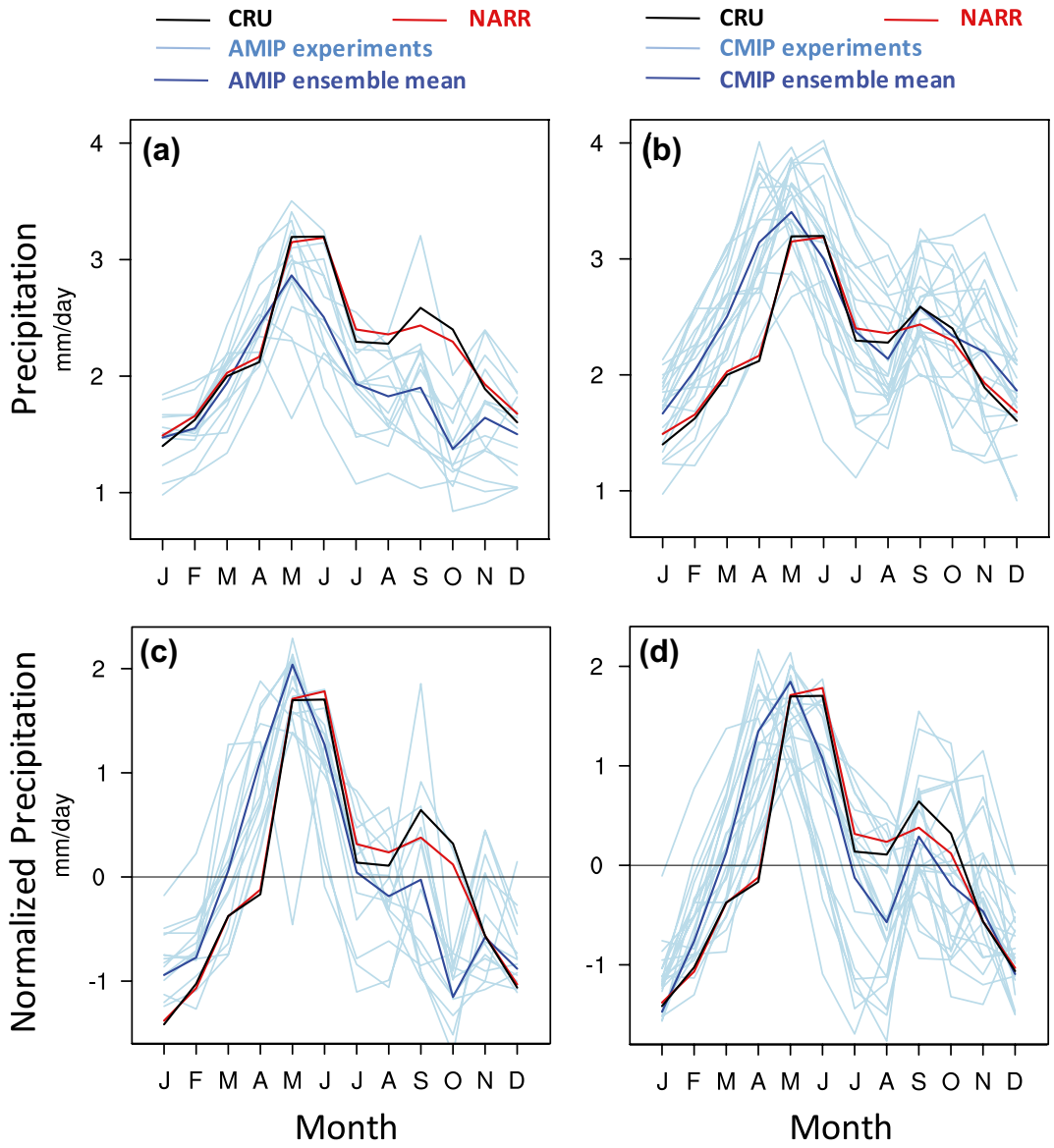

Fig. 3 Climatological (1979–2008) annual precipitation averaged over the SC region derived from **a** 14 AMIP simulations and **b** 22 CMIP simulations. Individual model simulations are plotted in *light blue* and multi-model ensembles are plotted in *blue*, while the *black* and *red lines* correspond to CRU and NARR data, respectively. Normalized annual precipitation cycles from **c** AMIP and **d** CMIP simulations are also shown

throughout the year except during the warm season (Fig. 4c, d). EW models, which have a wet bias during July and August, also tend to have a cold bias during the same months (Fig. 4d), while BM models that have a dry bias during July and August also have a slight warm bias or are comparable to the observed data (Fig. 4c). This implies that the observed inverse relationship between the surface temperature and precipitation during warm season is reasonably simulated in both EW and BM CMIP models; further evidence for this correlation between precipitation and temperature biases is provided in the Supplementary Information. In the next section, we will continue to explore possible causes for model bias, focusing on large-scale dynamical features such as the NASH and GPLLJ.

3.3 Relationship to the GPLLJ and the NASH

Large-scale dynamical features such as the NASH and GPLLJ are associated with moisture flux convergence and divergence as well as with the promotion and suppression of vertical motion, all of which affect the occurrence and magnitude of precipitation across the South Central U.S. Since these features occur at spatial and temporal scales consistent with the resolution of reanalysis and global

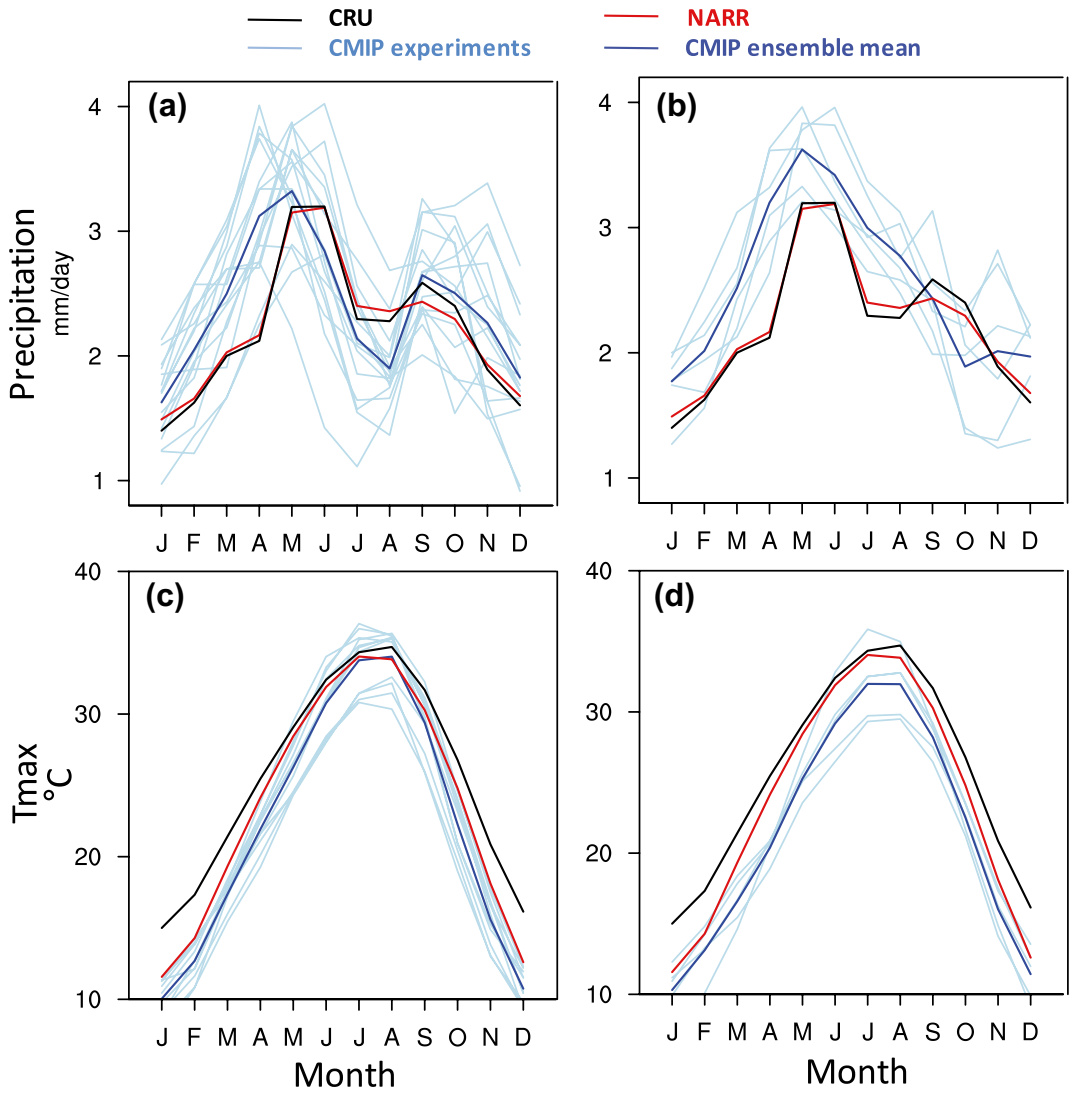

Fig. 4 Climatological (1979–2008) annual precipitation (*top*) and temperature (*bottom*) annual cycles averaged over the SC region from **a** 16 "BM" and **b** 6 "EW" models

climate model output, we next examine model ability to simulate the magnitude and variability of these features, as well as their potential role in driving both observed precipitation variability and the precipitation biases in both BM and EW CMIP5 models described above.

In Fig. 5, we use meridional wind at 925 hPa (shaded) and the 700 hPa geopotential height (contoured) to capture the month-to-month variations in the GPLLJ and the NASH during the wet season from April to September. In May, the GPLLJ begins to strengthen in the southern part of the domain; this enhanced GPLLJ and its meridional gradient can drive moisture transport from the Gulf of Mexico and moisture flux convergence in the SC region throughout May and June (see Supplementary Information), contributing to the first and largest precipitation peak in the wet season across the region (Mo et al. 2005). At the same time, the NASH begins to extend westward over the region, stalling over the southern U.S. in July and August. Its dampening influence on convection (Myoung and Nielsen-Gammon 2010) accounts for the mid-summer dry period observed across the region, as a high pressure system, large-scale subsidence, and relatively warm conditions above the convective boundary layer suppress convective activity, as well as possibly preventing mesoscale convective systems that develop over the Rocky Mountains from passing across the SC region. Towards the end of the summer, the NASH begins its eastward retreat while the GPLLJ begins to weaken, both factors that likely contribute to a second, smaller peak in precipitation in September.

In Fig. 6, we compare present-day NARR climatology of meridional wind at 925 hPa (again shaded) and geopotential height at 700 hPa (contoured) with the composite

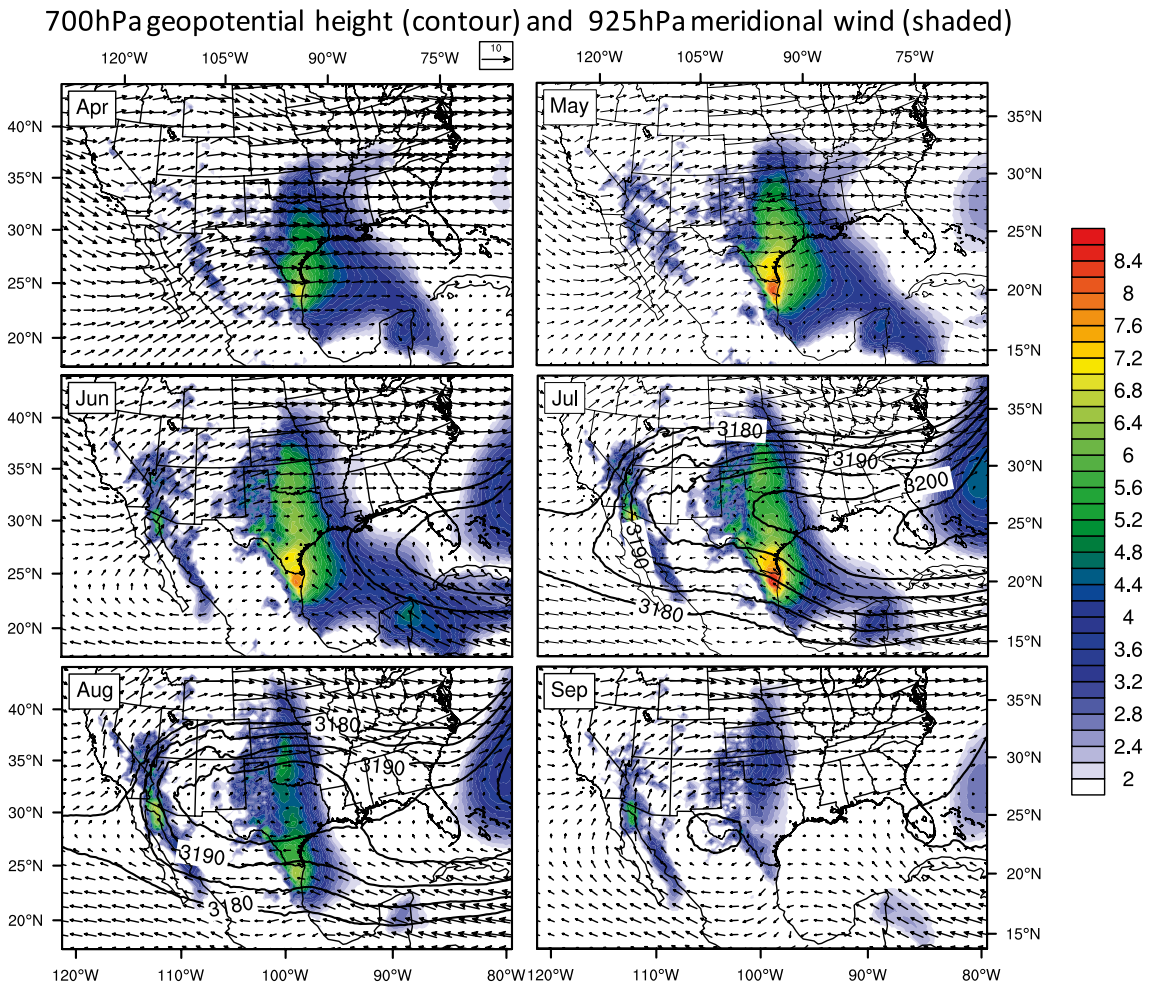

Fig. 5 Climatological monthly means of 700 hPa geopotential height (*black*, contoured) and 925 hPa meridional wind (*shaded*), and wind vectors at 700 hPa (*arrows*) from April to September based on NARR reanalysis

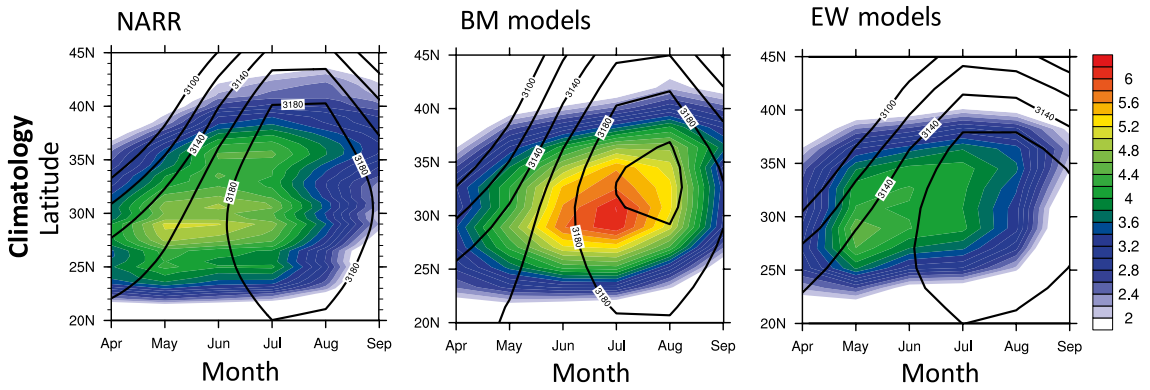

Fig. 6 Present-day climatology of the monthly mean geopotential height at 700 hPa (*contoured*) and meridional wind at 925 hPa (*shaded*) averaged over longitude between 103°W and 92°W from the NARR (*left*) and the multi-model ensemble means from CMIP5 "BM" models (*center*) and "EW" models (*right*)

of the BM and EW model groups, with values averaged over the longitude range between 103°W and 92°W. Compared to NARR, both groups of CMIP models are able to reproduce the basic characteristics of how the GPLLJ and the NASH shift over the year: in early summer, the GPLLJ strengthens south of 28°N while the NASH expands over the region; after summer, the jet quickly weakens and the NASH retreats. At the same time, there are some important differences between NARR and CMIP models, and between the two groups of CMIP models themselves. The first difference relates to the GPLLJ. NARR shows GPLLJ to be strongest around 28°N in May and June. The EW models show a peak in GPLLJ around 28°N at the correct time (i.e. May and June) although the amplitude is somewhat weak. In the BM models, the GPLLJ peaks later, from June to July, and its overall magnitude is too strong even in August. The BM models' bias in the timing and northward extension of the GPLLJ during summer, which presumably enhances moisture flux divergence, would logically result in the dry bias discussed previously. The second difference between NARR and CMIP models relates to the NASH. BM models simulate the westward extension of the NASH at the correct time, although the simulated NASH is slightly stronger than observed in July and August. This likely explains why the BM models *do* produce a bimodal pattern, as well as why every BM model's mid-summer dry period has even less precipitation than observed (Fig. 4a). In addition, in the BM models, the NASH tends to stall over the region in September, rather than moving out quickly as it does in NARR. This continued presence of the NASH over the region could explain the BM models' tendency towards a weaker-than-observed second precipitation peak in late summer as well. In the EW models, the westward extension of the NASH again occurs at the correct time, but is much weaker than observed during the summer, suggesting that—as hypothesized earlier—simulated circulation is not strong enough to suppress precipitation to the extent that would create a mid-summer dry period.

4 Contributions of the NASH and GPLLJ to summer drought

In the previous section, we showed how the mid-summer dry period that punctuates the wet growing season over the South Central region is likely related to the westward extension of the NASH over the region in July and August that tends to suppress convective precipitation during those months. We also showed how the ability of CMIP models to simulate this annual precipitation cycle is closely related to the simulated strength of the westward extension of the NASH over the region in summer. The GPLLJ is related to the primary wet season in May and June through moisture transport from the Gulf of Mexico and the moisture flux convergence over the SC region. Its meridional gradient seems to be reasonably simulated in both the BM and the EW models, except for the overestimation of the GPLLJ in July by the BM models. Given the relationship between the NASH, the GPLLJ, and summer precipitation over the region, we now examine the role these large-scale features may play during warm season drought both in NARR output and as simulated by CMIP5 models.

4.1 Observed and simulated historical droughts

To examine the pattern of large-scale circulation associated with observed and modeled drought years, we first identified historical dry years from gridded CRU precipitation data covering the period 1979 to 2012 to span the range of NARR output. This period also includes the droughts of the 1980s and 2010s. Dry years were identified by averaging seasonal (June–July–August) precipitation anomalies over the entire SC region (Fig. 1, red box) and normalizing them to zero mean and unit variance. Defining a dry year as occurring when the standardized anomaly is less than −1 identifies 5 dry years over the 30-year period: 1980, 1983, 1984, 2011 and 2012. Dry years in CMIP models were identified in the 30-year period 1979–2008 using the same approach. The number of dry years varies from three to six, depending on the models, and occurs in different years in

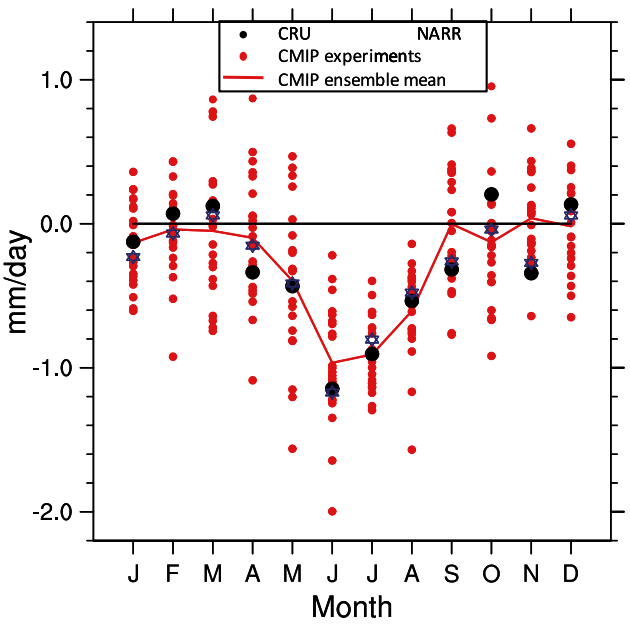

Fig. 7 Composite means of monthly precipitation anomalies averaged over the SC region for dry summers. *Red dots* indicate individual CMIP5 historical simulations and the *red line* represents the multi-model ensemble mean, while the *black dot* and *blue star* represent CRU and NARR data, respectively

each simulation as the timing of drought is determined primarily by natural variability rather than external forcing.

Composite monthly precipitation anomalies for the dry years calculated from CRU observations, NARR, and the 22 CMIP models are shown in Fig. 7. The multi-model CMIP ensemble mean shows a similar pattern to the observational data in that the precipitation deficit is the largest in June, followed by July, although the actual deficits vary widely from one model to the next.

Since Patricola and Cook (2013a) show that precipitation changes (primarily in June) can be explained by stationary moisture flux convergence related to a strengthening of the GPLLJ, we further examine the behavior of the NASH and the GPLLJ during warm season drought by calculating vertically integrated moisture flux convergence (hereafter referred to as "moisture flux convergence"). Figure 8 shows the NASH (*contours*) and GPLLJ (*shaded*) anomalies in historical dry years with respect to present-day climatology side-by-side with moisture flux convergence derived from the monthly variables that represent stationary moisture flux convergences. To examine soil moisture effect due to land–atmosphere interaction, soil moisture content anomaly is also displayed in bottom panel of Fig. 8.

During dry years, the GPLLJ is stronger and its northward extension during June—the driest month of the dry years—is much greater in the NARR analysis. A stronger and broader GPLLJ would act to increase moisture divergence and hence reduce precipitation over the SC region. In addition, the NASH is stronger and although its westward extension over the region occurs at the same time in early summer, in dry years it remains over the region through September. This implies the presence of a semi-permanent high pressure system over the region from June through September that would contribute to suppressing convective activity by large-scale subsidence in the upper-level atmosphere accompanied by intensification of the NASH's western ridge. Li et al. (2012) showed that the 850 hPa geopotential height anomaly of the western ridge of the NASH is closely related to the 500 hPa vertical pressure velocity anomaly. During historical dry summers, soil moisture deficits increase across the SC region and persist in late summer, a pattern that is reproduced by both BM and EW models. As addressed in previous studies (Trenberth et al. 1988; Koster et al. 2004, 2009), reduced precipitation is strongly linked to soil moisture deficit through both land–atmosphere interaction as well as large-scale circulation. In other words, meteorological drought is closely related to agricultural drought in the SC region due to the sensitivity of evaporation to soil moisture in a drier regime (Koster et al. 2009).

Are CMIP models able to reproduce the observed differences between dry years and the climatological average? Yes: both the BM and the EW models simulate a stronger GPLLJ with the northward extension during dry years, although the simulated enhancement of the GPLLJ tends to be underestimated in June, particularly by BM models that have stronger GPLLJ than the climatological average (Fig. 6). Associated with the strengthening of the GPLLJ with northward extension, both BM and EW models also simulate the increase in the moisture flux divergence across the SC region in June and July. In addition, the simulated westward extension of the NASH western ridge in the early summer and its intensification across the SC region throughout the summer resembles the anomaly patterns of precipitation in each group of models. However, it is interesting to see that the intensification of the NASH western ridge over the SC is overestimated in August by the EW models that simulate a weaker NASH western ridge and consequently fail to simulate the mid-summer dry period in the climatological average. The deficit of soil moisture dominating over the SC region (to the south of 40°N) and persisting throughout late summer is also reasonably simulated by both groups of the models.

In drought years, both BM and EW models are able to reproduce the observed combined influence of a stronger GPLLJ that reaches further north and a strengthened NASH western ridge, and are also able to reproduce the impact of these dynamical changes on precipitation throughout the summer. In other words, CMIP models are able to consistently reproduce the relationship of large-scale dynamical features and warm season drought over the South Central region, regardless of model ability to reproduce the behavior of these features on an annual basis and their impact on the climatological annual cycle of the precipitation over the region. This result builds confidence in model ability to simulate the large-scale characteristics of regional drought, while also raising critical questions regarding the utility of weighting models based on climatological performance when generating future projections of long-term trends.

4.2 Future projections

Future projections of precipitation for the South Central region show little change in annual average precipitation, but a consistent increase in summer dry conditions or drought (Walsh et al. 2014; Swain and Hayhoe 2015). Could this change be related to shifts in the NASH and/or GPLLJ that—as indicated above—occur in the historical record and are largely reproduced by CMIP models?

To answer this question, we compare projected changes in summer precipitation over the SC region with projected change in the NASH and GPLLJ under global mean temperature thresholds of +1, +2 and +3 °C relative to 1971–2000. As Fig. 8 indicates, while the sign and the magnitude of precipitation change varies from one model

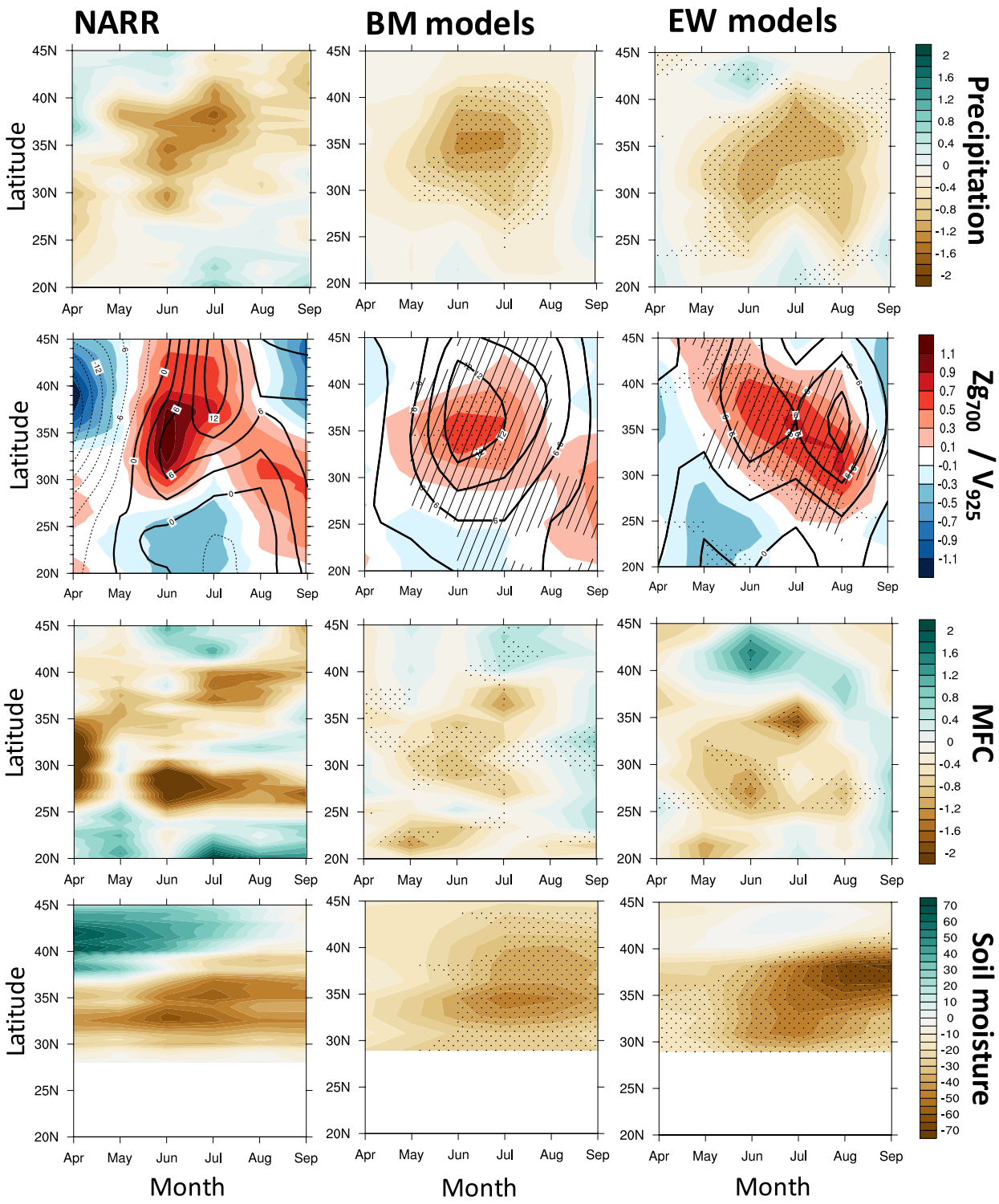

Fig. 8 Composites of historical dry summer's monthly mean anomalies in precipitation (mm day^{-1}, *top*), geopotential height at 700 hPa (m, *contoured*) and meridional wind at 925 hPa (m s^{-1}, *shaded*) (*second panel*), vertically integrated moisture flux convergence (mm day^{-1}, *third panel*), and soil moisture content (kg m^{-2}), averaged over longitude between 103°W and 92°W from the NARR (*left*) and the multi-model ensemble means from CMIP5 BM models (*center*) and EW models (*right*). Stippling with dots (precipitation, 925 hPa meridional wind, and soil moisture) and lines (700 hPa geopotential height) indicates where more than 75% (60%, for moisture flux convergence) of the simulations used to create the composite map agree on the sign of the multi-model ensemble mean changes

to the next throughout the year, as the world warms, the multi-model ensemble mean shows a tendency towards drier conditions in June and July, offset by an increase in March and April. Furthermore, this pattern of increased precipitation in early spring and decreased rainfall in mid-summer strengthens, as global mean temperature increases. Converting the multi-model average absolute values to percentages shows that, on average, precipitation is projected to decrease (increase) by up to 10% of the present climatological monthly value in July (April) under a global mean temperature increase of 3 °C (not shown).

Although the models tend to agree on these seasonal changes, agreement does not necessarily imply truth. What light can this analysis shed on the possible credibility of these projections? In terms of the projected increase in April precipitation, one regional climate modeling study (Patricola and Cook 2013a) suggested that it is related to the enhanced daytime convection. On the other hand, CMIP models tend to have a wet bias in April in the historical simulations (Fig. 3). Hence, we can't exclude the possibility that the projected increase in April precipitation might be related to the combined effects of a too-strong model response to surface heating in spring, combined with an increase in atmospheric moisture content due to warming of surface air. The extent to which this bias relates to surface heating and therefore the extent to which the projected increase in spring precipitation over the South Central region may be an artifact of this bias is an important question that remains to be investigated in future work. In contrast, the projected decrease of summer precipitation occurs during a time when models *are* able to simulate the impact of large-scale circulation on monthly precipitation and, as discussed previously in Sect. 3, their precipitation biases (including a too-strong mid-summer dry period in the BM models and a too-wet period in the EW models) appear to be linked to their ability to reproduce the annual (although not interannual) variability of these large-scale features.

To investigate whether changes in the NASH and GPLLJ are related to the projected decrease in future precipitation over the SC region in June and July, we compare projected changes in the NASH and GPLLJ (Fig. 10) under a global temperature increase by 1 and 2 °C with those in the historical climatology. Individual model results used to generate the composites in Fig. 10 as well as Fig. 6 are provided in the Supplementary Information. Not as much upper-air output is available for future as compared to historical CMIP5 simulations; for that reason, Fig. 9 shows results from only 14 models, 10 from the BM group and 4 from the EW group based on both the RCP4.5 and RCP8.5 simulations.

Comparing the top and bottom panels of Fig. 10, it is immediately obvious that in both the BM and the EW model groups the NASH is projected to strengthen, remaining strongest in July and August, and the GPLLJ is also projected to intensify as the global temperature increases. This intensification is most notable in July, when the GPLLJ is already strongest in historical simulations and when it becomes even stronger during historical dry years. For a global temperature increase of 2 °C, the GPLLJ becomes as strong in June as it is in July, which could be the result of an earlier westward extension of the NASH (as can be seen by comparing the 3100 and 3200 m contours between historical and future simulations). Overall, projected changes

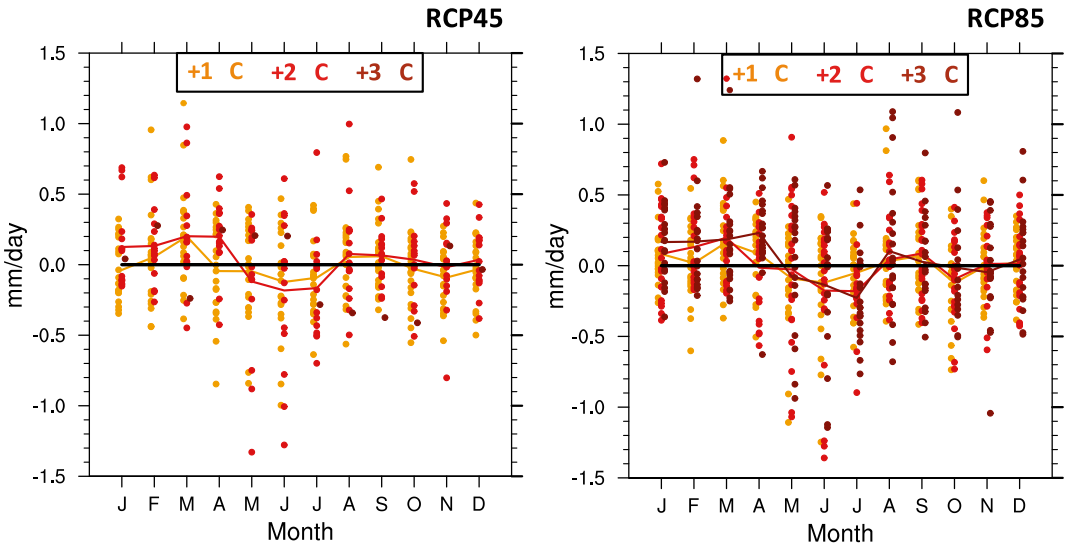

Fig. 9 Future changes of monthly precipitation over the SC region projected by the CMIP5 models under the RCP4.5 (*left*) and RCP8.5 (*right*) scenarios corresponding to global mean surface temperature increases of +1 °C (*blue*), +2 °C (*red*), and +3 °C (*purple*, for RCP8.5 only) relative to 1971–2000. *Dots* and *lines* represent individual models and multi-model ensemble means, respectively

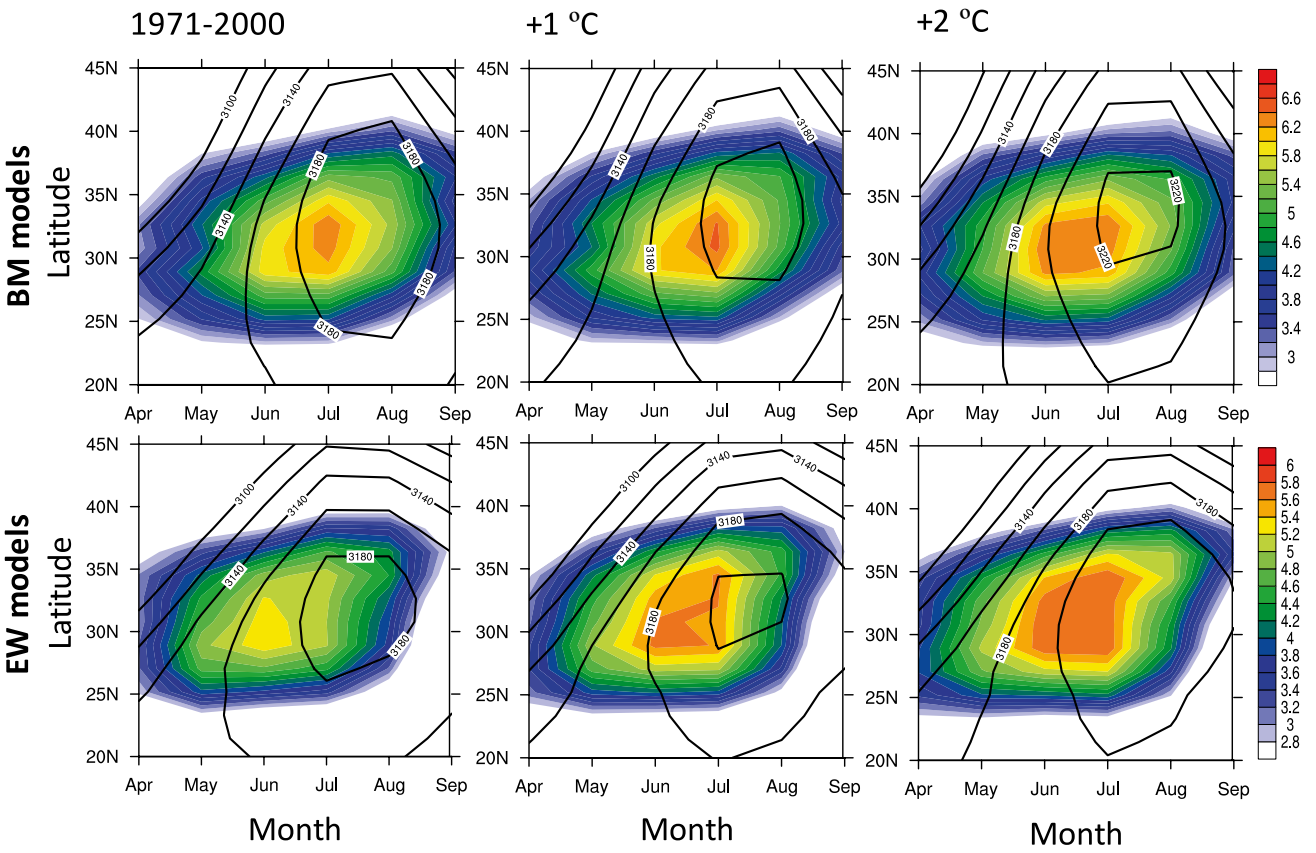

Fig. 10 The multi-model ensemble means of 700 hPa geopotential height (*contoured*) and 925 hPa meridional wind (*shaded*) averaged over the longitude range from 103°W to 92°W for 1971–2000 (*left*) and future projections corresponding to transient global mean surface temperature increases of +1 °C (*middle*) and +2 °C (*right*) relative to 1971–2000, respectively, for the CMIP5 BM models (*top*) and EW models (*bottom*)

in the GPLLJ seem to be closely related to changes in the NASH, and projected changes in both features—a stronger GPLLJ that extends northward and a stronger NASH that remains over the region through September—are similar to those observed and simulated during dry years in the historical period, and are consistent across both BM and EW models.

Projected changes in precipitation, 700 hPa geopotential height, 925 hPa meridional wind, moisture flux convergence, and soil moisture from historical climatology to mean conditions under a transient global temperature increase of 2 °C are presented in Fig. 11. The all-model ensemble mean shows a decrease in summer precipitation over the SC region (left, Fig. 11). Comparing the timing of these precipitation decreases with projected changes in the GPLLJ and moisture flux convergence, the June precipitation decrease appears concurrent with the strengthening and meridional extension of the GPLLJ that is in turn associated with an increase in moisture flux divergence, consistent with the results of Patricola and Cook (2013a). On the other hand, July and August precipitation decreases are concurrent with intensification of the NASH western ridge.

Comparing projected changes between the BM and EW model groups (middle and right, Fig. 11) shows that the BM models, those able to reasonably simulate the climatological mid-summer dry period in July and August, tend to project a precipitation decrease that is greatest in early summer (May–July), a decrease which appears to be associated with both moisture flux divergence from the northward extension of the GPLLJ as well as intensification of the NASH. In contrast, the EW models that fail to simulate the mid-summer dry period in the historical record tend to project a precipitation decrease that is greatest in late summer (July and August). This difference could explain why the projected change in precipitation over the SC region has a diverse distribution in Fig. 8, while the July precipitation change is more robust. Although the GPLLJ and the NASH begin to intensify in the early summer, their changes are greater in July and August. The resulting enhanced moisture flux divergence and the intensification of the NASH's

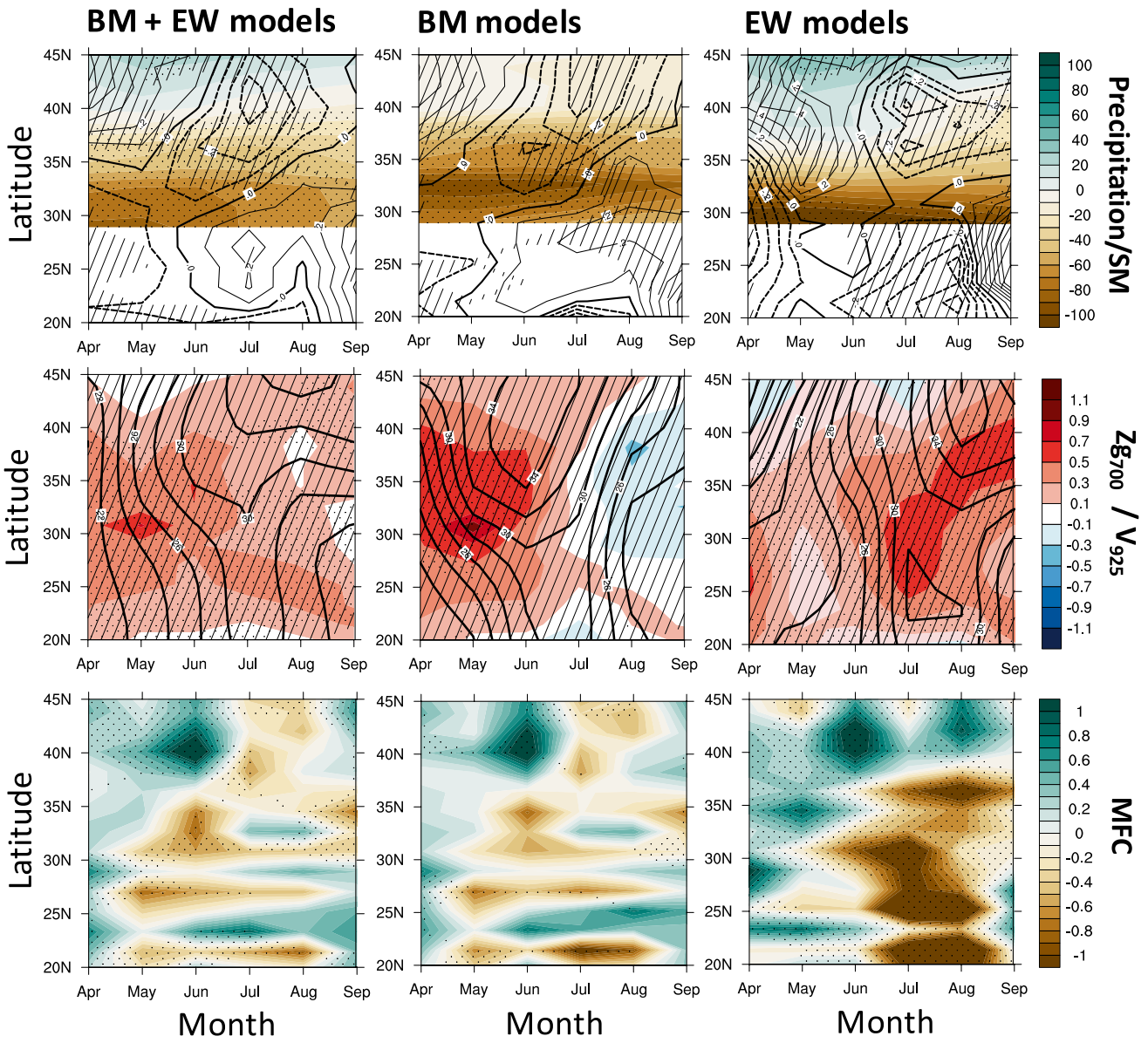

Fig. 11 Composites of projected future changes in (*top*) precipitation (mm day^{-1}, *contoured*) and soil moisture (kg m^{-2}, *shaded*), (*middle*) geopotential height at 700 hPa (m, *contoured*) and meridional wind at 925 hPa (m s^{-1}, *shaded*), and (*bottom*) vertically integrated moisture flux convergence (mm day^{-1}), averaged over longitude between 103°W and 92°W under a +2 °C transient global mean temperature change derived from RCP4.5 and RCP8.5 scenarios. Stippling with dots (925 hPa meridional wind, soil moisture, and moisture flux convergence) and lines (precipitation and 700 hPa geopotential height) is used to indicate where more than 60% of the models used in the composite agree on the multi-model ensemble means

western ridge drive the decrease in precipitation in July and August.

Projected soil moisture decreases in the SC region (mostly south of 40°N) due to near-surface warming is simulated by both BM and EW models, although BM models show more robust deficits, as land–atmosphere interactions modify the response to reduced early summer precipitation. These results emphasize the need for future work, beyond the scope of this study's focus on the influence of large-scale circulation on precipitation variability, to quantify the possible influence of land–atmosphere interactions on projected changes in soil moisture across the region.

5 Discussion and conclusions

Understanding the relationship between large-scale circulation, precipitation, and drought in water-short areas such as the South Central U.S., and assessing the extent to which global climate models are able to reproduce these

relationships and predict the direction of future change, can provide valuable insight into the future of agriculture and water management in the region. In this study, we examined the relationship between the NASH, the GPLLJ, and summer precipitation and drought in observational and reanalysis data. We then assessed the extent to which the 22 CMIP5 models for which sufficient data were available were able to reproduce these relationships from month to month, and whether they were able to simulate the anomalies in large-scale circulation patterns observed during dry years.

Climatological precipitation over the SC region is characterized by a bimodal distribution with a primary wet season in May and June, and a second peak in September and October punctuated by a mid-summer dry period in July and August. The majority of the 22 models were able to capture the bimodal distribution; we designated these as "BM" models. A fewer but still significant number of models did not have a dry period but rather just one extended wet period throughout the summer; we called these "EW" models. Comparing large-scale circulation patterns in the BM and EW models, we found that the BM models were able to reasonably simulate the timing and amplitude of the westward extension of the NASH and the intensified GPLLJ during the warm season, whereas the EW models tended to underestimate the amplitude of the westward extension of the NASH and the GPLLJ, a factor that could explain their wet bias during summer.

During historical dry summers, both observations and historical simulations agree that the precipitation deficit occurs at the same time as a stronger NASH that remains over the region through September, rather than shifting back eastward in August as it does on average. Summer precipitation in dry years could also be affected by a stronger GPLLJ with a greater northward extension, observed in June but primarily simulated to occur in July. The stronger and longer NASH and the more intense and northward extended GPLLJ could contribute to a precipitation deficit over the SC region by creating unfavorable conditions for convective activity such as mid-tropospheric stability and moisture flux divergence. Regardless of whether they lie in the BM or the EW group, CMIP5 models are generally able to capture these anomalies in both monthly precipitation and large-scale circulation during dry years, with some small differences between the two groups (for example, that the enhanced GPLLJ tends to peak in July rather than in June, as observed).

Future projections under a range of global mean temperature thresholds, from +1 to +3 °C relative to the present climatology, suggest that precipitation across the South Central region is likely to decrease in summer, particularly in June and July. This decrease appears to be related to the combined influence of a stronger and longer-lasting NASH and an intensified GPLLJ—a similar pattern to what already occurs in both NARR reanalysis and historical simulations of extreme dry years. Both projected precipitation deficits and changes in the NASH and GPLLJ become more evident under greater amounts of warming.

In summary, this analysis suggests that projected decreases in summer precipitation over the region may be robust: future changes in warm-season precipitation and the large-scale circulation patterns that affect it appear to be similar to the observed and simulated historical relationships between warm-season drought and anomalous large-scale circulation. CMIP5 models are generally able to capture the anomalous intensification of the westward extension of the NASH, the intensification and northward extension of the GPLLJ, and the consequent moisture flux divergence that occurs during dry years, driving summer precipitation deficits in the historical record. This ability appears unrelated to model performance in simulating the annual cycle (i.e. whether the model falls into the BM or the EW group). However, *when* the projected precipitation deficits occur does appear to depend on model performance. In BM models, summer precipitation decreases are projected to be greatest in early summer (May–June), a result of anomalous large-scale circulation patterns extending over the region in a manner reminiscent of historical dry years. In EW models, on the other hand, future decrease in precipitation are projected to be greatest in late summer (July–August) when anomalous large-scale circulation patterns are projected to be dominant. Since our results imply that the NASH is closely related to the historical droughts as well as the future precipitation changes in the South Central U.S., in future work we plan to investigate how SC droughts could be affected by natural modes of climate variability such as the Pacific/North Atlantic (PNA) and the North Atlantic Oscillation (NAO) that affect multi-year NASH variability, as well as low-frequency variability of sea surface temperature in the Atlantic and Pacific Oceans, factors that have previously been shown to be related to the drought across the region (Hoerling and Kumar 2003; Schubert et al. 2004, 2009; Nigam et al. 2011; Seager et al. 2014; Harding and Snyder 2015; Patricola et al. 2015).

Acknowledgements We acknowledge the World Climate Research Programme's Working Group on Coupled Modelling, which is responsible for CMIP, and we thank the climate modeling groups (listed in Table 1 of this paper) for producing and making available their model output. For CMIP5 the U.S. Department of Energy's Program for Climate Model Diagnosis and Intercomparison provided coordinating support and led development of software infrastructure in partnership with the Global Organization for Earth System Science Portals. This research was supported by USGS Award Number G15AP00137.

References

Barandiaran D, Wang SY, Hilburn K (2013) Observed trends in the Great Plains low-level jet and associated precipitation. Geophys Res Lett. doi:10.1002/2013GL058296

Barriopedro D, Fischer EM, Lutenbacher J, Trigo RM, Garcia-Herrera R (2011) The hot summer of 2010: redrawing the temperature record map of Europe. Science 332(6026):220–224

Basara JB, Maybourn JN, Peirano CM, Tate JE, Brown PJ, Hoey JD, Smith BR (2013) Drought and associated impacts in the great plains of the United States—a review. Int J Geosci 4:72–81

Bechtold, Chaboureau JP, Beljaars A, Betts AK, K¨ohler M, Miller M, Redelsperger JL (2004) The simulation of the diurnal cycle of convective precipitation over land in a global model. Q J R Meteorol Soc 130:3119–3137

Betts A, Ball JH, Beljaars ACM, Miller MJ, Viterbo PA (1996) The land surface-atmosphere interaction: a review based on observational and global modeling perspectives. J Geophys Res 101:7209–7225

Blackadar AK (1957) Boundary layer wind maxima and their significance for the growth of nocturnal inversions. Bull Amer Meteor Soc 38:283–290

Bonner WD, Paegle J (1970) Diurnal variations in the boundary layer winds over the south-central United States in summer. Mon Wea Rev 98:735–744

Bukovsky MS, Karoly DJ (2007) A brief evaluation of precipitation from the North American Regional Reanalysis. J Hydrometeo 8:837–846

Chang FC, Wallace JM (1987) Meteorological conditions during heat waves and droughts in the United States Great Plains. Mon Wea Rev 115:1253–1269

Moss RH and coauthors (2010) The next generation of scenarios for climate change research and assessment. Nature 463:747–756

Cook KH, Vizy EK, Launer ZS, Patricola CM (2008) Springtime intensification of the Great Plains low-level jet and Midwest precipitation in GCM simulations of the twenty-first century. J Clim 21:6321–6340. doi:10.1175/2008JCLI2355.1

Dai A (2006) Precipitation characteristics in eighteen coupled climate models. J Clim 19:4605–4630

Davis RE, Hayden BP, Gay DA, Phillips WL, Jones GV (1997) The North Atlantic subtropical anticyclone. J Clim 10:728–744

Dickson RR (1980) Weather and circulation of June 1980-inception of a heat wave and drought over the central and southern Great Plains. Mon Wea Rev 108:1469–1474

Diem JE (2006) Synoptic-scale controls of summer precipitation in the Southeastern United States. J Clim 19:613–621

Dirmeyer PA, Cash BA, Kinter III JL, Jung T, Marx L, Satoh M, Stan C, Hirofumi T, Towers P, Wedi N, Achuthavarier D, Adams JD, Altshuler EL, Huang B, Jin EK, Manganello J (2012) Simulating the diurnal cycle of rainfall in global climate models: resolution versus parameterization. Clim Dyn 39:399–418

Durre I, Wallace JM, Lettenmaier DP (2000) Dependence of extreme daily maximum temperatures on antecedent soil moisture in the contiguous United States during summer. J Clim 13(14):2641–2651

Fannin B (2012) Updated 2011 Texas agricultural drought losses total $7.62 billion. Texas A&M AgriLife Today. http://today.agrilife.org/2012/03/21/updated-2011-texas-agriculturaldrought-losses-total-7-62-billion/ March 21, 2012

Garfin G, Franco G, Blanco H, Comrie A, Gonzalez P, Piechota T, Smyth R, Waskom R (2014) Ch. 20: Southwest. In Climate change impacts in the United States: The third national climate assessment, edited by J.M. Melillo, T.C. Richmond, and G.W. Yohe. Washington, DC: U.S. Global Change Research Program, 462–486

Harding KJ, Snyder PK (2014) Examining future changes in the character of Central U.S. warm-season precipitation using dynamical downscaling. J Geophys Res 119:13116–13136. doi:10.1002/2014JD022575

Harding KJ, Snyder PK (2015) The relationship between the Pacific–North American Teleconnection Pattern, the Great Plains Low-Level Jet, and North Central U.S. Heavy Rainfall Events. J Clim. doi:10.1175/JCLI-D-14-00657.1

Harding KJ, Snyder PK, Liess S (2013) Use of dynamical downscaling to improve the simulation of Central U.S. warm season precipitation in CMIP5 models. J Geophys Res 118:12522–12536. doi:10.1002/2013JD019994

Harris I, Jones PD, Osborn TJ, Lister DH (2014) Updated high-resolution grids of monthly climatic observations – the CRU TS3.10 Dataset. Int J Climatol 34:623–642

Helfand HM, Schubert SD (1995) Climatology of the simulated Great Plains low-level jet and its contribution to the continental moisture budget of the United States. J Clim 8:784–806

Henderson KG, Muller RA (1997) Extreme temperature days in the south-central United States. Clim Res 8:151–162

Henderson KG, Vega AJ (1996) Regional precipitation variability in the southern United States. Phys Geogr 17:93–112

Higgins RW, Yao Y, Yarosh ES, Janowiak JE, Mo KC (1997) Influence of the Great Plains low-level jet on summertime precipitation and moisture transport over the Central United States. J Clim 10:481–507

Hoerling M, Coauthors (2013) Anatomy of an extreme event. J Clim 26:2811–2832

Hoerling M, Kumar A (2003) The perfect Ocean for Drought. Science 299:691–694

Holton JR (1967) The diurnal boundary layer wind oscillation above sloping terrain. Tellus 19:199–205

Hoxit LR (1975) Diurnal variations in planetary boundary-layer winds over land. Bound Layer Meteor 8:21–38

Klein WH (1952) The weather and circulation of June 1952-A month with a record heat wave. Mon Wea Rev 80:99–104

Koster RD (2004) Regions of strong coupling between soil moisture and precipitation. Science 305:1138–1140

Koster RD, Schubert SD, Suarez MJ (2009) Analyzing the concurrence of meteorological droughts and warm periods, with implications for the determination of evaporative regime. J Clim 22:3331–3341

Kutzbach JE (1967) Empirical eigenvectors of sea-level pressure, surface temperature and precipitation complexes over North America. J Appl Meteor 6:791–802

Li W, Li L, Fu R, Deng Y, Wang H (2011) Changes to the North Atlantic subtropical high and its role in the intensification of summer rainfall variability in the southeastern United States. J Clim 24:1499–1506

Li L, Li W, Kushnir Y (2012) Variation of North Atlantic Subtropical High western ridge and its implication to the southeastern US summer precipitation. Clim Dyn 39:1401–1412

Li L, Li W, Jin J (2015) Contribution of the North Atlantic subtropical high to regional climate model (RCM) skill in simulating southeastern United States summer precipitation. Clim Dyn 45:477–491

Madden RA, Williams J (1978) The correlation between temperature and precipitation in the United States and Europe. Mon Wea Rev 106:142–147

Mesinger et al (2006) North American Regional Reanalysis. Bull Amer Meteor Soc 87:343–360. doi:10.1175/bams-87-3-343

Mo KC, Chelliah M, Carrera ML, Higgins RW, Ebisuzaki W (2005) Atmospheric moisture transport over the United States and Mexico as evaluated in the NCEP regional reanalysis. J Hydrometeo 6:710–728

Myoung B, Nielsen-Gammon (2010) The convective instability pathway to warm season drought in Texas. Part II: free-tropospheric modulation of convective inhibition. J Clim 23:4474–4488

Namias J (1955) Some meteorological aspects of drought with special reference to the summers of 1952-54 over the United States. Mon Wea Rev 83:199–205

Namias J (1982) Anatomy of Great Plains Protracted Heat Waves (especially the 1980 U.S. summer drought). Mon Wea Rev 110:824–838

NCDC (2013) Billion-dollar weather/climate disasters 1980–2016. Available online: http://www.ncdc.noaa.gov/billions/events.pdf. Accessed 16 Sept 2013

Nigam S, Guan B, Ruiz-Barradas A (2011) Key role of the Atlantic Multidecadal Oscillation in 20th century drought and wet periods over the Great Plains. Geophys Res Lett 38:L16713. doi:10.1029/2011GL048650

Ortegren JT, Knapp PA, Maxwell JT, Tyminski WP, Soule PT (2011) Ocean-atmosphere influences on low-frequency warm-season drought variability in the Gulf coast and Southeastern United States. J Appl Meteorol Climatol 50:1177–1186

Patricola CM, Cook KH (2013a) Mid-twenty-first century climate change in the Central United States. Part I: regional and global model predictions. Clim Dyn 40:551–568

Patricola CM, Cook KH (2013b) Mid-twenty-first century climate change in the Central United States. Part II: climate change processes. Clim Dyn 40:569–583

Patricola CM, Chang P, Saravanan R (2015) Impact of Atlantic SST and high frequency atmospheric variability on the 1993 and 2008 Midwest floods: regional climate model simulations of extreme climate events. Clim Change 129:397–411

Rodwell MJ, Hoskins BJ (2001) Subtropical anticyclones and summer monsoon. J Clim 14:3192–3211

Ruiz-Barradas A, Nigam S (2005) Warm-season rainfall variability over the U.S. Great Plains in observations, NCEP and ERA-40 reanalyses, and NCAR and NASA atmospheric model simulations. J Clim 18:1808–1830

Ruiz-Barradas A, Nigam S (2013) Atmosphere-land-surface interactions over the Southern Great Plains: characterization from pentad analysis of DOE-ARM Field observations and NARR reanalysis. J Clim 26:875–886

Ryu J-H, Hayhoe K (2014) Understanding the sources of Caribbean precipitation biases in CMIP3 and CMIP5 simulations. Clim Dyn 42:3233–3252. doi:10.1007/s00382-013-1801-1

Seager R, Goddard L (2014) Dynamical causes of the 2010/11 Texas-Norther Mexico drought. J Hydrometeo 15:39–69

Shafer M, Ojima D, Antle JM, Kluck D, McPherson RA, Petersen S, Scanlon B, Sherman K (2014) Ch. 19: Great Plains. Climate Change Impacts in the United States: The Third National Climate Assessment, Melillo JM, Richmond TC, Yohe GW, Eds., U.S. Global Change Research Program, 441–461. doi:10.7930/J0D798BC

Schubert SD, Coauthors (2009) A U.S. CLIVAR Project to Assess and Compare the Responses of Global Climate Models to Drought-Related SST Forcing Patterns: Overview and Results. J Clim 22:5251–5272

Schubert SD, Surez MJ, Pegion PJ, Koster RD, Bacmeister JT (2004) Causes of long-term drought in the U.S. Great Plains. J Clim 17:485–503

Swain S, Hayhoe K (2015) CMIP5 projected changes in spring and summer drought and wet conditions over North America. Clim Dyn 44:2737–2750

Taylor KE, Stouffer RJ, Meehl GA (2012) An overview of CMIP5 and the experiment design. Bull Am Meteorol Soc 93:485–498

Ting M, Wang H (2006) The Role of the North American Topography on the Maintenance of the Great Plains Summer Low-Level Jet. J Atmos Sci 63:1056–1068

Trenberth KE, Branstaror GW, Arkin PA (1988) Origins of the 1988 North American Drought. Science 242:1640–1645

USDA FSA (2015) Secretarial Drought Designations - All Drought. United Stated Department of Agriculture Farm Services Agreement. Washington DC. Jan 28, 2015. http://www.usda.gov/documents/usda-drought-fast-track-designations-012815.pdf

Walsh J, Coauthors (2014) Ch. 2: Our changing climate. In Climate change impacts in the United States: The third national climate assessment, edited by Melillo JM, Richmond TC, and Yohe GW. Washington, DC: U.S. Global Change Research Program, 19–67

Weaver SJ, Nigam S (2008) Variability of the Great Plains low-level jet: large-scale circulation context and hydroclimate impacts. J Clim 21:1532–1551. doi:10.1175/2007JCLI1586.1

Weaver SJ, Nigam S (2011) Recurrent supersynoptic evolution of the Great Plains low-level jet. J Clim 24:575–582

Weaver SJ, Schubert S, Wang H (2009) Warm season variations in the low-level Circulation and precipitation over the Center United States in observations, AMIP Simulations, and idealized SST experiments. J Clim 22:5401–5420. doi:10.1175/2009JCLI2984.1

Wexler H (1961) A boundary layer interpretation of the low-level jet. Tellus 13:368–378

Wuebbles D et al (2014) CMIP5 climate model analyses: climate extremes in the United States. Bull Am Meteorol Soc 95:571–583

Zhao S, Deng Y, Black RX (2016) Warm Season Dry Spells in the Central and Eastern United States: diverging Skill in Climate Model Representation. J Clim. doi:10.1175/JCLI-D-16-0321.1